Test Results of Superconducting Combined Function Prototype Magnets for the J-PARC Neutrino Beam Line

Ken-ichi Sasaki, Tatsushi Nakamoto, Norio Higashi, Nobuhiro Kimura, Yasuo Ajima, Toru Ogitsu, Takayuki Tomaru, Masahisa Iida, Hirokatsu Ohhata, Shigekatsu Sugawara, Ken-ichi Tanaka, Yasuhiro Makida, Takahiro Okamura, Osamu Araoka, Katsuyu Kasami, Akira Yamamoto

***Abstract*— Superconducting combined function magnets are adopted for the 50 GeV, 750 kW proton beam line for the J-PARC neutrino experiment, and two full-scale prototype magnets have been developed successfully at KEK. In the cold tests, the both prototypes was excited up to 7700 A without a spontaneous quenches. The measured field quality of the both prototypes agreed well with the design field, indicating that the fabrication process has no major problem. The heater quench tests of the first prototype, however, showed that the magnet was not self-protected. Based on the safety design revised, quench protection heaters were adopted as an additional protection scheme. In heater quench tests of the second prototype magnet using small sheet heaters, the fundamental characteristics of the quench protection heaters were studied.**

***Index Terms*— J-PARC, Neutrino, Superconducting Combined Function Magnet, Magnetic Field Measurement, Quench Protection Heater.**

I. Introduction

A next generation long-baseline neutrino oscillation experiment is planned to study fundamental nature of neutrinos [1], [2]. It will require the proton beam extracted from J-PARC 50 GeV, 0.75 MW proton accelerator jointly built by JAERI and KEK. The beam line which guides the proton beam to the production target of secondary particles consists of 28 superconducting combined function magnets, SCFMs, currently developed at KEK.

The unique feature of the magnet design is a left-right asymmetric structure. A cross section of the magnet and an enlarged view of the half coil are shown in Fig 1. The magnets have a large aperture of 173.4 mm, a magnetic length of 3.3 m and an outer diameter of 570 mm. The current distribution which generates both dipole field of 2.6 T and quadrupole field of 19 T/m with a current of 7345 A, is combined into a single layer coil. The coil is encased in the glass-fiber reinforced phenolic plastic collars surrounded by an iron yoke. The yoke design is based on the CERN-LHC IR Quadrupole magnet, MQXA, developed at KEK [3]. The use of the plastic collar instead of conventional metallic collars and the design transferred from MQXA contributes to reduce fabrication costs.

Two full-scale prototypes of SCFMs have been developed successfully at KEK. The first prototype magnet is to confirm the magnet design and fabrication tools, and the second prototype magnet is to verify the technology transfer to an industrial company and the reproducibility of manufacturing process. The details on the design and development of SCFMs are described in the previous papers [4]-[7]. This paper reports the results of cold tests of the first and second prototype magnets. In addition, the revision of quench protection scheme is reported.

II. Results of Excitation Tests

The cold test was performed in a liquid helium of 4.2 K in a vertical cryostat with an inner diameter of 720 mm and a depth of 9 m, which was used for testing of LHC-MQXA magnets. Fig. 2 shows the installtion of the magnet into the vertical cryostat. After the first cold test, the first prototype magnet was once warmed up to room temperature, then, cooled again and the second cold test was carried out.

In the first prototype magnet the magnet was ramped up at 5 A/s and successfully reached 7700 A, the current limit of the power supply, without a spontaneous quenches, after nine manually switched-off tests at the power supply current gradually increased for checking the system. It sufficiently exceeds the operational current of 7345 A at the expected maximum proton beam energy of 50 GeV. The fast ramp tests up to the nominal current of 7345 A were also conducted with different ramp rates, although the magnet will be operated only on DC mode. The magnet did not quench even at the maximum ramp rate of 1000 A/s corresponding to the ramp rate limit of the power supply, indicating that AC loss in the magnet is small. During the fast ramp up/down tests, the inductance of the magnet was measured. The inductance derived from inductive voltage of the magnet was about 14.2 mH which is consistently close to the design value of 14.3 mH.

After the first cold test, the first prototype was once warmed up to room temperature, and cooled down again. In the second cold test, the magnet was energized up again to 7700 A without spontaneous quenches, and other test results were the same as that in the first cold test. Namely, no thermal cycle effect was observed on the magnet performance.

Manuscript received September 20, 2005.

Ken-ichi Sasaki, Tatsushi Nakamoto, Norio Higashi, Nobuhiro Kimura, Yasuo Ajima, Toru Ogitsu, Takayuki Tomaru, Masahisa Iida, Hirokatsu Ohhata, Shigekatsu Sugawara, Ken-ichi Tanaka, Yasuhiro Makida, Takahiro Okamura, Osamu Araoka, Katsuyu Kasami and Akira Yamamoto are with the High Energy Accelerator Research Organization (KEK), 1-1 Oho, Tsukuba, 305-0801 Japan (e-mail:ken-ichi.sasaki@kek.jp).

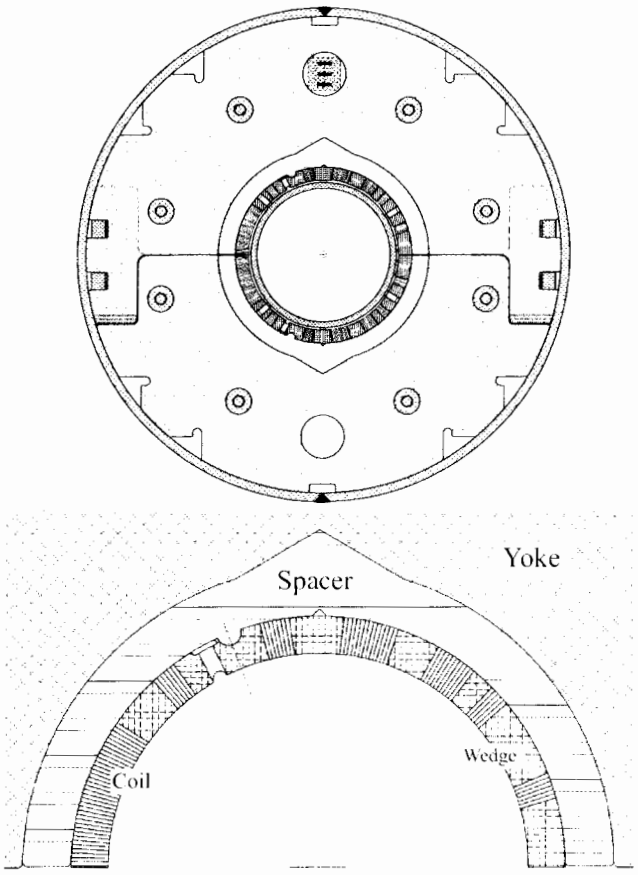

Fig. 1. Cross section of the superconducting combined function magnet viewed from head end (top), and enlarged view of the coil (bottom). The coil aperture diameter is 173.4 mm.

In the second prototype magnet, the same excitation tests as the first prototype, were carried out. The second prototype was energized to the current of 7700 A without a spontaneous quench, too. The fast ramp tests were also conducted, and the magnet experienced the first spontaneous quench at 6453 A. This magnet didn't have the voltage taps to identify the position of quench origin, therefore, it can be only found that the quench started in the lower half of the coil cross section. However, the magnet is limited to DC application, so it does not affect on the basic magnet performance. The magnet inductance measured during the fast ramp tests was about 14.3 mH, corresponding the design value.

III. Magnetic Field Measurement

A. Measurement System

The magnetic field measurements were performed with a rotating probe. The rotating probe consists of five radial coils with rectangular shape about 20 mm wide and 500 mm long that are printed and placed in parallel on a circuit board by an etching method. Each coil has 20 turns. The rotating probe can move along the magnet axis in the warm bore of the vertical cryostat for scanning the magnet axis. Analog bucked signals to reduce dipole and/or quadrupole components were taken by using a precise digital integrator, that was triggered by an angular encoder. The harmonics field is derived from Fourier coefficients of readouts of integrator.

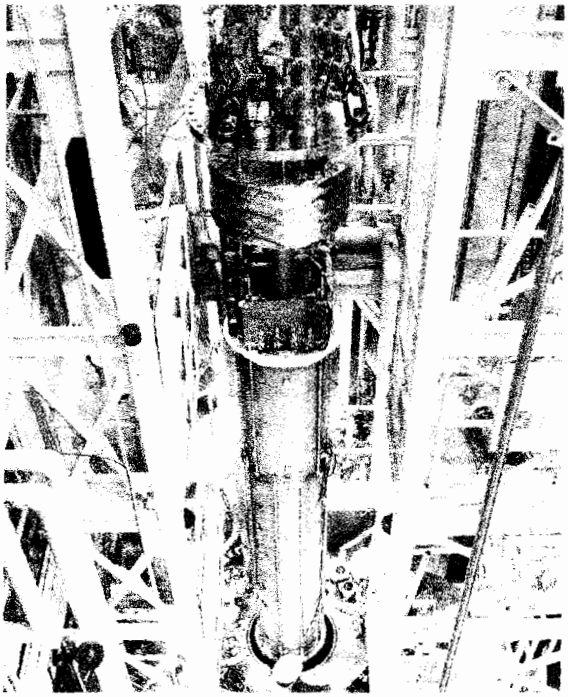

Fig. 2. Prototype magnet installation into the vertical cryostat.

B. Definition of Multipole Components

The multipole components are described as the multipole coefficients on a reference radius, r_0, of 50 mm by the equation 1.

$$B_y + iB_x = \sum_{n=1}^{\infty} (B_n + iA_n) \left(\frac{x + iy}{r_0} \right)^{(n-1)} \quad (1)$$

where B_n, A_n are the normal and the skew 2n-pole field (in Tesla).

A main concern about the field measurement of combined function magnets, is the position of the rotating axis of the probes. The magnet is hanged in a vertical cryostat during the individual cold test, and it is very difficult to coincide the axis of rotation with the magnet central axis. This fact makes it difficult to determine the dipole field with good accuracy in the SCFM. Because SCFM generates both the dipole and quadrupole fields, and "feed down" of quadrupole field affects on the amplitude of dipole signal. In the following analysis, the angular compensation is only adopted so that the skew quadrupole component along the straight section might be fit into zero. The exact dipole field will be measured at the horizontal test stand for the several production magnets. The warm measurement at the horizontal test bench are reported in [8].

C. Results

Table I summarizes the field qualities in the magnet straight section at 40 GeV and 50 GeV. The measured results are

TABLE I
FIELD QUALITY OF THE SCFM IN THE STRAIGHT SECTION AT THE REFERENCE RADIUS OF 5 CM

Multipole	Measured @5921 A	Measured @7460 A	Computed @5830 A	Computed @7345 A
B_1(T)	2.14	2.68	2.069	2.586
B_2(T)	0.76	0.95	0.753	0.936
$B_3(10^{-4}\mathrm{T})$	9.3	16.5	4.0	4.3
$B_4(10^{-4}\mathrm{T})$	0.3	25.6	0.5	23.4
$B_5(10^{-4}\mathrm{T})$	− 5.4	0.2	1.9	6.5
$B_6(10^{-4}\mathrm{T})$	14.4	−19.6	12.3	−16.2
$B_7(10^{-4}\mathrm{T})$	− 7.3	11.6	1.0	− 2.3
$B_8(10^{-4}\mathrm{T})$	−18.0	24.5	7.7	9.8
$B_9(10^{-4}\mathrm{T})$	20.2	−25.7	−18.4	23.0
$B_{10}(10^{-4}\mathrm{T})$	− 3.8	5.1	− 0.5	0.7
$B_{11}(10^{-4}\mathrm{T})$	− 3.0	3.1	− 6.0	7.9
$B_{12}(10^{-4}\mathrm{T})$	4.9	6.2	4.2	5.3

TABLE II
INTEGRAL FIELD QUALITY OF THE SCFM AT THE REFERENCE RADIUS OF 5 CM

Multipole	Measured @5921 A	Measured @7460 A	Computed @5830 A	Computed @7345 A
B_1(T·m)	7.097	8.906	6.954	8.712
B_2(T·m)	2.510	3.127	2.501	3.120
$B_3(10^{-4}\mathrm{T\cdot m})$	187.1	220.6	236.7	293.6
$B_4(10^{-4}\mathrm{T\cdot m})$	− 68.4	− 5.9	64.9	20.1
$B_5(10^{-4}\mathrm{T\cdot m})$	59.2	51.9	− 41.0	− 30.6
$B_6(10^{-4}\mathrm{T\cdot m})$	− 55.8	− 75.2	48.4	62.8
$B_7(10^{-4}\mathrm{T\cdot m})$	− 29.8	− 44.6	− 14.8	20.9
$B_8(10^{-4}\mathrm{T\cdot m})$	− 54.9	− 74.5	− 25.2	− 32.0
$B_9(10^{-4}\mathrm{T\cdot m})$	62.9	− 79.9	− 58.4	− 73.4
$B_{10}(10^{-4}\mathrm{T\cdot m})$	10.1	13.8	0.3	− 0.3
$B_{11}(10^{-4}\mathrm{T\cdot m})$	− 9.9	− 10.9	− 20.3	− 25.5
$B_{12}(10^{-4}\mathrm{T\cdot m})$	18.9	13.2	13.2	16.6

compared with the computed results in Table I. The computation is made using Opera2D. The measured field strength of the quadrupole field is in good agreement with computation, although there is small discrepancy in dipole field. It may be induced by the alignment error of the measurement system with respect to the magnet center as described above. The estimated alignment error is about 2.5 mm, which is presumable from the measurement system tolerances. The change in higher-order multipole coefficient from 40 GeV to 50 GeV is small except for the octupole coefficient consistently observed in the measured results.

The integral field quality of the magnet is summarized in Table II. The computed results are obtained using Opera3D. The measured results generally agree with computed results. Since the field quality around the coil ends is not as good as that in the straight section due to limited optimization of the single layer coil structure, the magnitude of higher order harmonics was relatively large. However, the beam simulations indicate that such field quality is good enough for the primary proton beam line extracted for the J-PARC neutrino experiment.

The field measurements of the second prototype were performed using the same system as the first prototype. The field qualities in the straight section and integrated field of the second prototype magnet are given in Fig. 3 and 4, respectively. The figures in parentheses represent dipole and quadrupole components. In the both straight section and integral field, there were no major discrepancy between the first and second prototype, which disturbed the beam transportation. This indicates that the reproducibility of the fabrication of the magnet are good enough, and the fabrication technology is smoothly transferred.

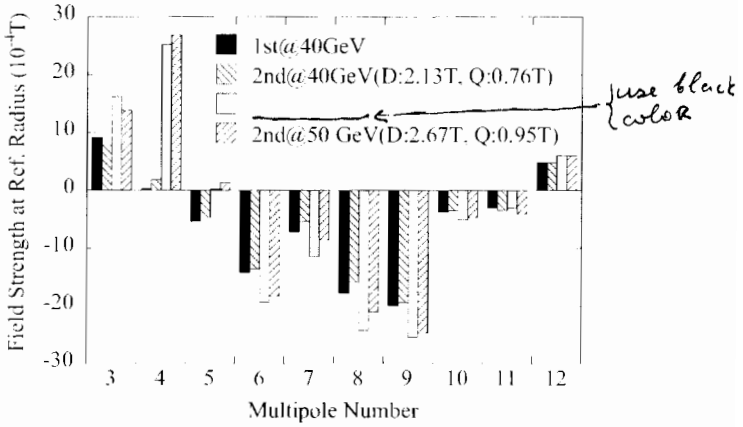

Fig. 3. Field strength at the reference radius of 5 cm of the second prototype magnet. The results of the first prototype magnet are also plotted for comparison. The figures in parentheses represent dipole and quadrupole components at 5920 A and 7460 A.

IV. HEATER QUENCH TESTS

A. Results of the First Prototype

The first prototype magnet is equipped with 57 voltage taps and 6 quench-inducing heaters to observe the quench characteristics. The magnetic field distribution on the conductors is asymmetry due to its unique coil structure, the field on the left side is higher than the right side in Fig. 1. The quench-inducing heaters are attached to the both top and bottom coils at three positions; at the 7th turn of the high field side, 36th turn in the low field side, and at the lead end on the median plane in the lowest field region. These heaters can induce quench in a single cable. The voltage taps are mainly attached around the heaters so that the initial quench propagation can be observed. In the quench tests, the dump resistor of 50 mΩ instead of the cold diode was connected in parallel to the coil circuit. The power supply was shut down when the magnet balance voltage exceeded a threshold of the quench detector.

The balance voltage rises of the magnet at currents of 7345 A and 5830 A are shown in Fig. 5. The voltage rise, when the heater at the lower field was fired, was much slower than the higher field. This is caused by the difference of quench propagation velocity at each magnetic field. Fig. 6 shows the quench propagation velocities as a function of distance from quench heater. The symbol represents the average quench propagation velocity within the section divided by dotted lines. The velocity in the lower field region is very slow, especially, the velocity around the lead is about 2 m/s, mainly because of the large quench margin of the cable. The calculated magnetic field around the heater at the lead is about 0.8 T at 7345 A, the I/Ic ratio is expected to be only about 0.04.

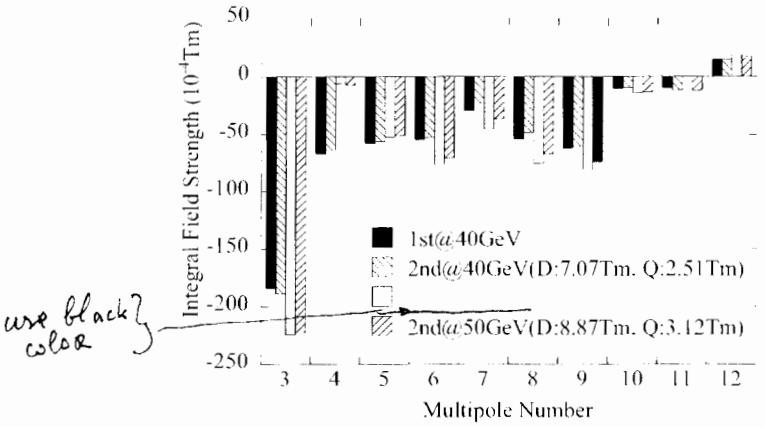

Fig. 4. Integral field quality at the reference radius of 5 cm of the second prototype magnet. The results of the first prototype magnet are also plotted for comparison. The figures in parentheses represent dipole and quadrupole components at 5920 A and 7460 A.

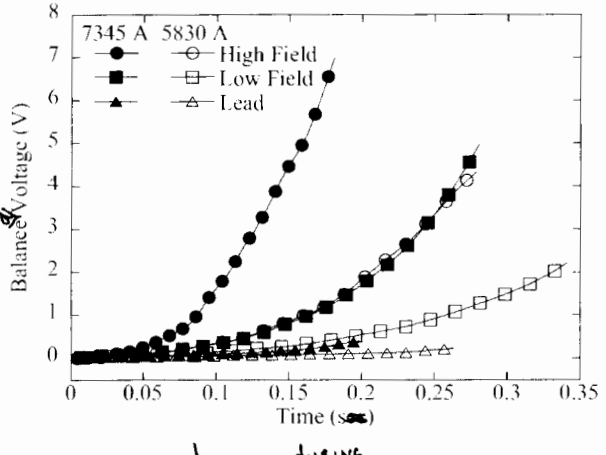

Fig. 5. Measured balance voltage rise at the heater quench tests at the currents corresponding to 50 GeV and 40 GeV. t = 0 s is the start time of the quench.

B. Numerical Simulation of Quench Protection

In the initial protection scheme, the magnets are protected by only the cold diode connected in parallel to each magnet [5]. Under a normal operating condition, the diode is cooled to the liquid helium temperature, and the turn on voltage of the diode is expected to be 6 V. The magnet voltage is considerably lower than the turn-on voltage, therefore, the current does not flow into the diode. Once the quench occurs and propagates, the magnet terminal voltage exceeds the turn-on voltage eventually, and current bypasses to the cold diode. The cold diode is warmed up by the bypassing current, and the forward voltage of the diode decreases with the temperature rise. The reduction of the forward voltage enhances the current bypass and eventually prevent the magnet from the overheating. However, the voltage developments observed in the cold tests of the first prototype magnet were crucially slow as described in the previous section. In order to re-evaluate the quench protection scheme, the numerical simulation was carried out.

1) Simulation Model: The basic equation to simulate the magnet quench is the one-dimensional thermal equilibrium

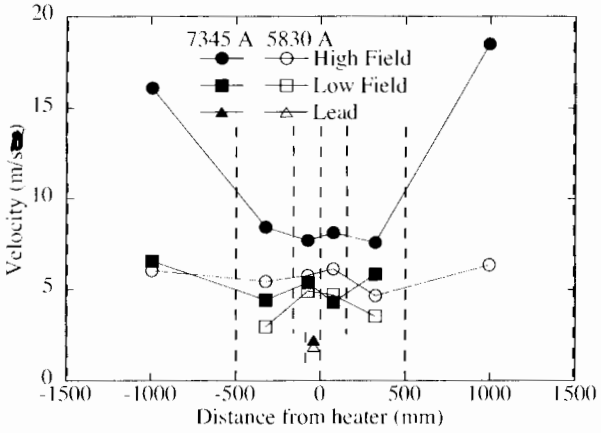

Fig. 6. Measured quench propagation velocity at the nominal current of 50 and 40 GeV.

equation as follows:

$$\frac{\partial}{\partial x}\left(\kappa(T)\frac{\partial T}{\partial x}\right) + g + p_{cn} = C(T)\frac{\partial T}{\partial t}. \qquad (2)$$

where κ is the thermal conductivity, T is the temperature, g is the heat generation per unit volume, p_{cn} is the heat conduction between the cables, and C is the specific heat. This equation is solved along the cable step by step with the Crank-Nicholson method. Other simulation conditions are as follows: the plastic spacer and G11 wedge is thermally insulated, no heat conduction between the top and bottom coils, the cold diode is connected in parallel with the magnet, and the magnet is under adiabatic conditions. The fourth condition is not actual because the magnet system will be cooled by a supercritical helium, however, such severe estimation seems to be preferable with respect to the quench protection study.

2) Numerical Results: First, the simulation was carried out in the same condition as the heater quench tests of first prototype except for connecting the cold diode instead of the dump resistor. Fig. 7 shows the temperature profile in the magnet at 1.0 s after the quench. The quench initiates at the center of the straight section at the high field side. The normal zone does not propagate in the magnet so much, and the maximum temperature exceeds 500 K. Such high temperature is not acceptable for quench protection. It is no wonder that the peak temperature in the quench at lower field is higher than the quench at high field. Fig. 8 shows the current changes and maximum temperatures in the magnet. In the quench at lower field, the quench propagation is slow and the bypass of current into the cold diode is delayed, therefore, the temperature rises steeply.

Comparison of the numerical results with the test results are shown in Fig. 9, which shows the resistive voltage of both the numerical and test results at different quench positions. The computation voltage at the higher field is much lower than the test results in spite of the adiabatic condition. These discrepancies are seemed that the conditions of computation are not optimized for the test results. However, the calculated result almost agreed with measured one at the lowest field, where is the most severe region in terms of the quench protection.

The calculated temperature in that condition is over 700 K in Fig. 8. It cannot be expected that the cooling effect helps to reduce the peak temperature by several hundred Kelvin. These results indicate that the SCFM is not self protected with the cold diode.

3) Discussion of Quench Protection Scheme: The three additional quench protection methods were examined by the computation; a) use copper wedges in the coil straight section instead of the G11 wedges, b) cover the outside of the coil straight section with high purity aluminum sheet, and c) attach quench protection heaters, QPHs. Fig. 10 shows the current and temperature changes in the three cases of the quench at the lowest field. The maximum temperatures of Al sheets slightly decrease in comparison with the no additional protection scheme, because of the enhancement of the thermal propagation by the Al sheets. However, the temperature is still too high. In the case of the Cu wedges, they don't help the peak temperature decrease at all. Meanwhile, the calculation for the quench protection heaters shows a good result. This computation was made assuming that the small sheet heater covering 21 turns in the width of 80 mm is attached at the lead end of the straight section of the top and bottom coils. The quench detector is needed for the method. The computation was made at the threshold of 0.1V, 20 ms. The peak temperature decreased to an acceptable value in terms of the magnet protection. These results show that the quench protection heater is adequate for the SCFM safety protection.

Some more simulations assuming the QPH method were carried out. Fig. 11 shows the relation between the peak temperature and the delay from the quench initiation until the QPH causes further quench. The computations were made in the case of two QPHs and four QPHs. The former is placed at the lead end of straight section of the both top and bottom coils, and the latter is placed the both lead and return end of the straight section of the both coils. The delay of thermal diffusion of the QPH through the thermal insulation is expected to be about 0.1 s. Considering the difficulty of the detection of the quench due to the electrical noise, 4 QPHs are preferable for the safe protection.

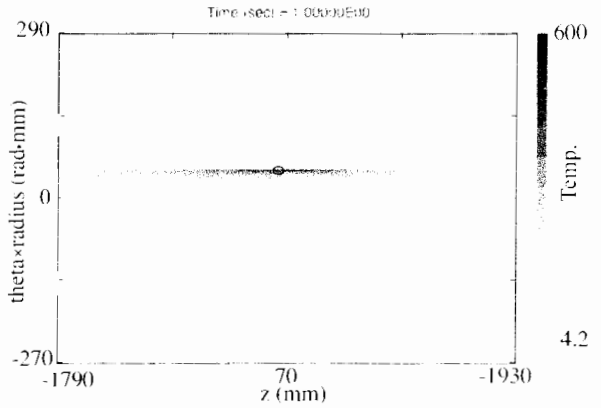

Fig. 7. The calculated temperature profile in 1.0 s after the quench. The quench initiates at the center of the straight section at the high field side, pointed by a open circle.

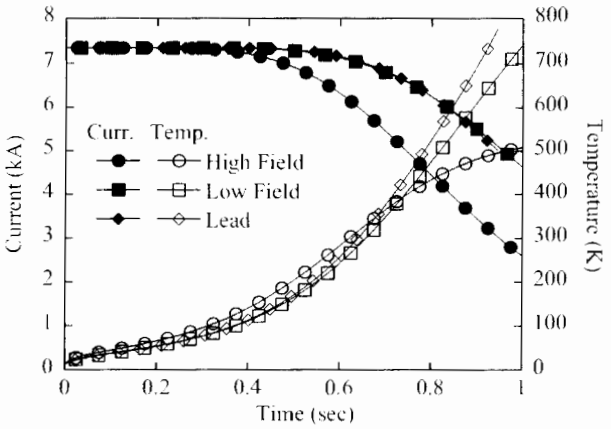

Fig. 8. The current and temperature changes in the case of the quench at the higher field, lower field and lead.

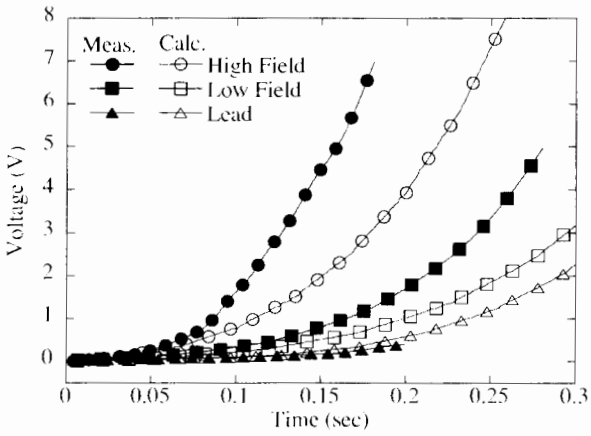

Fig. 9. The calculated and measured voltage developments at 50 GeV.

C. Test Results of the Second Prototype

The second prototype magnet has two QPHs at the lead end of the straight section in the higher field. The end spacers made of G11 were grooved with the rectangular shape in the depth of 0.3 mm, and the small sheet heaters, 66 mm wide × 44 mm height, were set in the grooves with the Kapton tape which controls the total thickness.

The important information of the QPH is the input energy required to initiate the quench. The heater covers several turns of the coil, and it must cause the quench in all the turns at once. Fig. 12 shows the balance voltage rise at the different heater energies. The magnet current was 5830 A. The voltage signal with about 50 J closely resembled the signal with 63 J. It indicates that the energy density of more than 0.017 J/mm^2 is needed to initiate the quench in all the turns covered by the QPH. In these tests, the time delay from the start of the heater pulse until the quench initiation was about 0.19 s at least, which was defined by the total thickness of the thermal insulation between QPH and the cable which was about 0.33 mm in this magnet. In the production magnets, the thickness of the insulation will be reduced to about 0.18 mm so that the time delay is expected to be about 0.1 s. As described in the previous section, the total time delay up to 0.26 s is acceptable in terms of the magnet protection.

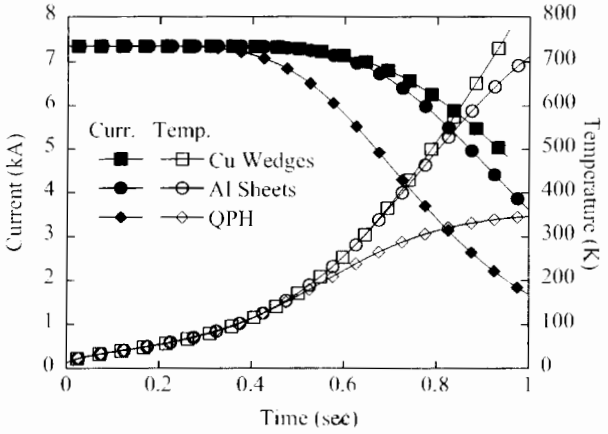

Fig. 10. The current and maximum temperature changes assuming the Al sheets, Cu wedges and quench protection heaters. The quench initiates at the lead on the median plane.

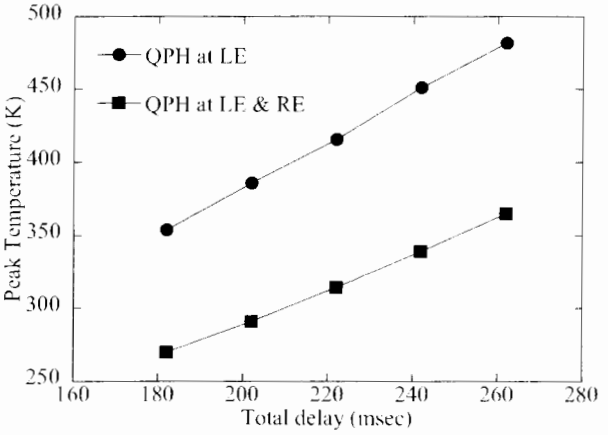

Fig. 11. The calculated peak temperature as a function of total delay.

therefore, the threshold of the quench detector can be selected conservatively.

V. Summary and Further Plan

Two full-scale prototypes of SCFMs for the primary proton beam line of the J-PARC neutrino experiment were tested at 4.2 K. In the excitation tests, both magnets were successfully energized up to 7700 A without spontaneous quenches. The first prototype magnet did not degrade at all after the thermal cycle. In the field measurement of both prototypes, the field quality in the straight section and the integrated field along the magnet axis almost met the specifications, except for the dipole field, which was not measured exactly in the present vertical testing system. The heater quench tests of the first prototype showed that the quench propagation velocity in the lower field region was much slower than expected, and the revision of the quench protection scheme was needed. The simulation results indicated that the only quench protection heater can protect the magnet. It was also found from the computation that the four small QPHs were enough to prevent the magnet from burnout. In the second prototype magnet, the heater quench tests using the small sheet heaters were performed, and the effective energy density of the QPH was derived from the comparison of the balance voltages at the different heater energies.

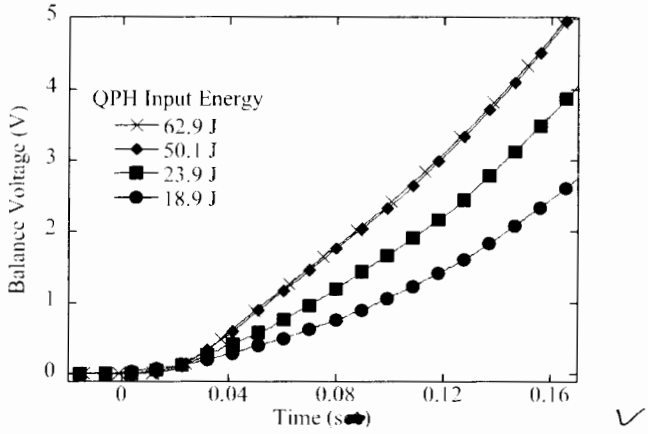

Fig. 12. The balance voltages at different heater energies when the quench was induced by the QPH on the bottom coil.

The first prototype magnet has been disassembled after the second test, and four quench protection heaters have been attached in the identical positions to those which are planned for the production magnet. The reassembled prototype magnet is to be tested soon again in the vertical cryostat. The two prototype magnets are to be integrated as a pair of magnet system with a prototype horizontal cryostat being developed, and the full test will be carried out in the horizontal position in early 2006.

References

[1] Y. Itow et. al., "The JHF-Kamioka neutrino project," hep-ex/0106019.
[2] M. Furusaka, R. Hino, Y. Ikeda *et. al.*, "The joint project for high intensity proton accelerators," KEK Report 99-1; JAERI-Tech 99-056; JHF-99-3, 1999.
[3] Y. Ajima, *et al.*, "The MQXA quadrupoles for the LHC low-beta insertions," *Nucl. Inst. Method* A550(2005), 499-513.
[4] T. Nakamoto, N. Higashi, T. Ogitsu *et. al.*, "Design of Superconducting Combined Function Magnets for the 50 GeV Proton Beam Line for the J-PARC Neutrino Experiment," *IEEE Trans. on Appl. Superc.* Vol. 14, No. 2 (2004) 616 - 619.
[5] T. Ogitsu, Y. Makida, T. Kobayashi *et al.*, "Superconducting Magnet System at the 50 GeV Proton Beam Line for the J-PARC Neutrino Experiment," *IEEE Trans. on Appl. Superc.* Vol. 14, No. 2 (2004) 604 - 607.
[6] T. Nakamoto, *et al.*, "Development of a Prototype of Superconducting Combined Function Magnet for the 50 GeV Proton Beam Line for the J-PARC Neutrino Experiment," to be published in *IEEE Trans. Appl. Superconduct.*, Vol.15, 2005.
[7] T. Nakamoto, Y. Ajima, Y. Fujii *et al.*, "Development of Superconducting Combined Function Magnets for the Proton Transport Line for the J-PARC Neutrino Experiment," Proc. of Particle Accelerator Conference 2005.
[8] T. Tomaru, K. Sasaki, T. Nakamot *et al.*, "Alignment and warm measurements of the J-PARC combined function magnets," to be presented at this conference, MOA08PO02.